J|A|C|S
COMMUNICATIONS

Published on Web 11/02/2004

Attaching Organic Semiconductors to Gate Oxides: In Situ Assembly of Monolayer Field Effect Transistors

George S. Tulevski,[†] Qian Miao,[†] Masafumi Fukuto,[‡] Rebecca Abram,[†] Benjamin Ocko,[‡] Ronald Pindak,[‡] Michael L. Steigerwald,[†] Cherie R. Kagan,*[,§] and Colin Nuckolls*[,†]

Contributions from the Department of Chemistry and the Nanoscience Center, Columbia University, New York, New York 10027; Brookhaven National Laboratory, Upton, New York 11970; and IBM T.J. Watson Research Center, Yorktown Heights, New York 10598

Received September 28, 2004; E-mail: cn37@columbia.edu

Detailed below is a new tetracene derivative (**1**) that forms dense, upright monolayers on the surface of aluminum oxide (Figure 1b). These monolayers spontaneously self-organize into the active layer in nanoscale field-effect transistor devices (Figure 1c) when aluminum oxide is used as the dielectric layer.[1] This method gives high yields of working devices that have source-drain distances that are less than 100 nm and provides a new avenue for research in thin-film organic transistors where the active molecules are linked to the dielectric surface.

Linear acenes, such as pentacene and tetracene, have been heavily studied for molecule-based electronics due to their relatively high field effect mobilities and large ON/OFF current ratios when incorporated into TFTs.[2−5] The motivation for this study was a number of reports showing that in organic thin-film devices the first few molecular layers of organic semiconductor are the locus of charge injection and responsible for current modulation.[6−14] The rigid, covalent attachment detailed here provides a direct method for using the dielectric surface structure as an adjustable parameter to tune the monolayers' self-assembled structure and therefore their electrical properties.

The molecular design is illustrated in Figure 1a. It consists of a tetracene molecule (**1**) that has one of its terminal rings functionalized as a catechol. The *ortho*-hydroxyl functionality was chosen, since it is known to chelate a variety of metal oxides via a mononuclear bidentate coordination.[15−19] Although the use of catechols to form monolayers on the surface of aluminum oxide appears to be unprecedented, previous studies both on aluminum oxide nanoparticles and in organometallic complexes indicate catechols dehydrate with aluminum oxide to form a rigid, five-membered aluminum ester (Figure 1b).[15−19]

Reports of end functionalized linear acene syntheses are rare, apparently due to their difficulty in synthesis.[20,21] Here we devised a new and general synthesis (shown in Scheme 1) that provides the substituted tetracene derivatives. The key step utilizes a Diels−Alder cyclization to couple two easily prepared pieces: the exocyclic diene[22,23] (derived from the in situ loss of sulfur dioxide from the cyclic sulfinate ester **2**) and the 6,7-dimethoxy naphthoquinone **3**.[24,25] Instrumental for a clean synthesis is the intermediate reduction of the quinone to the tetrone. Reduction to the acene followed by unmasking of the hydroxyl groups with boron tribromide provides the target structure. Tetracene **1** is readily soluble in solvents such as diethyl ether, THF, DMF, DMSO, and acetone.

From solution in THF, **1** was screened against a number of oxide surfaces,[26] revealing binding to the surface of HfO_2, ZrO_2, Y_2O_3, and Al_2O_3. The assembly on aluminum oxide was investigated further because aluminum oxide is a common gate oxide material and its crystals (e.g., sapphire) are readily available. Detailed below are the results from our studies to understand the monolayer assembly of **1** using synchrotron X-ray reflectivity, reflection−absorption infrared spectroscopy (RAIRS), and X-ray photoelectron spectroscopy (XPS).

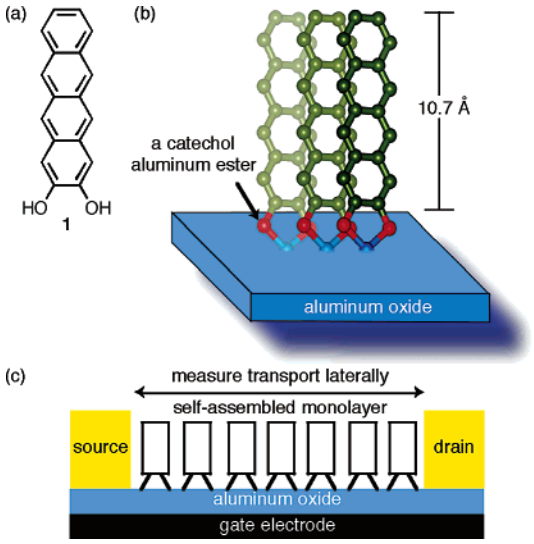

Figure 1. (a) End functionalized tetracene **1**. (b) Schematic of bonding and orientation of **1** on aluminum oxide (not intended to indicate in-plane ordering). (c) Schematic of the self-assembled monolayer transistor.

Scheme 1. Synthesis of **1**[a]

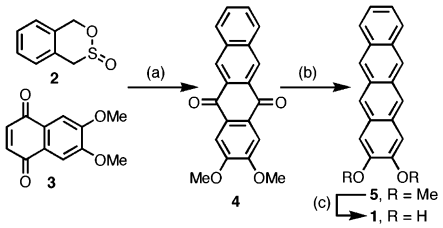

[a] key: (a) (*i*) Δ; (*ii*) Br_2, pyridine; (b) (*i*) Pd/C, H_2, TsOH; (*ii*) $LiAlH_4$ then H^+; (c) BBr_3.

The synchrotron X-ray reflectivity measurements, sensitive to changes in the laterally averaged electron density across interfaces, reveal that the molecules are upright and tightly packed in the monolayer. Figure 2a shows the normalized X-ray reflectivity data taken of the monolayer of **1** on the *c*-plane (0001) of a sapphire crystal using synchrotron radiation.[27] Plotted along with the normalized data is a fit to the data, calculated by assuming a single layer[28] of uniform density on top of the substrate.[29,30] Three

[†] Columbia University.
[‡] Brookhaven National Laboratory.
[§] IBM T.J. Watson Research Center.

10.1021/ja044101z CCC: $27.50

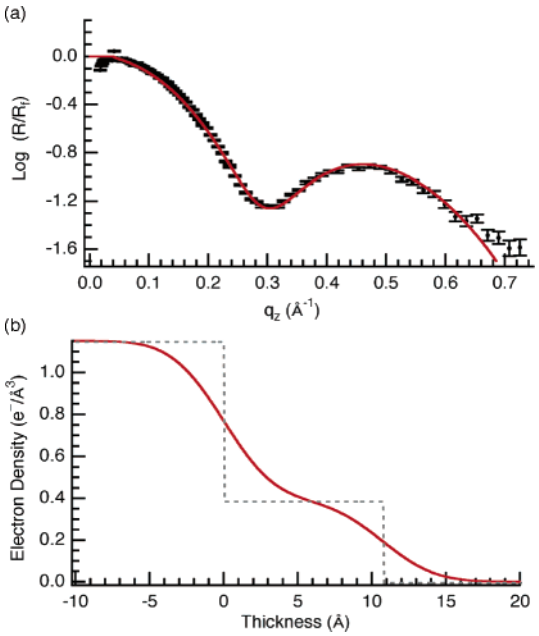

Figure 2. (a) Normalized X-ray reflectivity curve (black dotted curve) for SAM of **1** on aluminum oxide crystal surface along with plot of the data fit (solid red line). (b) Electron density profile (red) using fit data from Figure 2a along with box diagram (dashed gray) illustrating thickness and electron density with roughness equal to zero.

parameters are allowed to vary during the fit: the thickness, the electron density of the over-layer, and a common surface roughness for both the substrate/monolayer and monolayer/air interfaces.[31] Figure 2b is the electron density profile generated with the best-fit parameters and represents the surface in real space. From analysis of the reflectivity data the monolayer has a thickness of 10.7 ± 0.2 Å and an electron density of 0.389 ± 0.015 e$^-$/Å^3. Remarkably, the value for the electron density of the tetracene[33] crystal can be back calculated and is found to be 0.393 e/Å^3 indicating that the molecules in the monolayer are nearly as tightly packed as those in the bulk crystal.

The calculated height (approximately 10.7 Å, shown in Figure 1b) is identical with the length of the molecules measured in the X-ray reflectivity measurements. This similarity is a strong indication that the molecules are essentially upright. The calculated height assumes that catechol oxygens are now incorporated into the sapphire crystals through dehydration.[32] The two important observations for the electronic properties of these monolayers are that the molecules adopt a preferred upright conformation and are densely packed.

Angle-resolved X-ray photoelectron spectroscopy (XPS) was used to probe the core electron binding energies of the atoms present on the surface of the aluminum oxide. The angle dependent spectra are consistent with an aromatic carbon overlayer on the aluminum oxide surface. The C/Al ratio increases with decreasing takeoff angle, adding further support to the model that has a hydrocarbon based monolayer on top of the substrate.[34] Moreover, there was no evidence in the XPS spectra that the catechol had oxidized to an orthoquinone.[35]

The results from the RAIRS spectra of monolayers of **1** compared to the bulk (KBr pellet) support the conclusions from the reflectivity and XPS measurements[36] and also allow the nature of the bonding to the surface to be probed. The most striking difference between the bulk and the monolayer spectra is the frequency shift in the νC═C aromatic ring stretch (from 1500 cm^{-1} in bulk to 1465 cm^{-1} in the monolayer). In oxide nanoparticles and films, this shift has been attributed to deprotonation of the hydroxyl groups giving a bidentate chelation.[15,16,37] This double surface attachment drastically

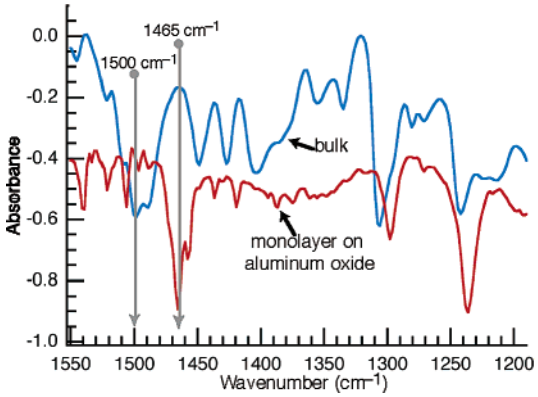

Figure 3. RAIRS spectra of a monolayer of **1** (red spectra) on aluminum oxide compared to a bulk sample (blue spectra) from a KBr pellet. The monolayer curve was shifted down by 0.4 absorbance units.

attenuates the frequency of the aryl ring stretching. Also seen in the IR comparison in Figure 3 is significant change in the resonance for νC—O stretch coupled to the δO—H bend.[15,16] This is due to the loss of δO—H bending mode during surface attachment. In the bulk sample this transition appears as a multiplet between 1250 and 1200 cm^{-1} that becomes a single stretch (1240 cm^{-1}) when **1** is assembled on the surface.

Another method to probe these monolayers is to measure their electronic properties. To this end, an electrical test bed for monolayer assembly was created. The devices, shown schematically in Figure 4a, have a thin layer (approximately 5 nm) of aluminum oxide deposited onto a 5 nm thermally oxidized, $n+$ doped silicon wafer. The aluminum oxide was utilized to act both as a dielectric layer and also as a primer for the assembly of **1**. Gold source and drain electrodes (200 Å, Au) were then patterned on these surfaces using e-beam lithography to have a source to drain separations between 30 and 100 nm, shown in Figure 4b,c. Widths of the devices were 250 nm. Assuming that each molecule occupies roughly 0.5 nm × 0.5 nm of area when assembled upright on a substrate, these test structures will probe small assemblies, on the order of 10 zeptomoles of material (i.e., $<10^4$ molecules).

For in situ monolayer assembly the test structures were immersed into a solution of **1** (in THF, 1×10^{-3} M, 12 h), removed, rinsed with fresh THF, dried under a stream of nitrogen, and probed electrically. A set of typical current−voltage curves as a function of gate bias are shown in Figure 4d for a device with $l = 40$ nm along with the AFM image from this device. Albeit not ideal transistor characteristics, the material behaves like a p-type, hole transporting semiconductor. The yield of devices that showed similar increase in source-drain current with applied gate bias was high for 60 nm or shorter devices (42 out of 80 devices tested) but dropped off sharply for devices with $l > 60$ nm. AFM images of the substrates with or without molecules show aluminum oxide grains around 40 nm in diameter. It seems likely that this grain structure would prevent transport in the larger test structures as it may give rise to poor contact between the monolayers on adjacent aluminum oxide grains. The nonlinear I/V curves and lack of current saturation[38−40] observed in Figure 4d may arise from high contact resistance, as assembly of tetracenediol is not expected on the Au electrode surface and may provide a barrier to charge injection. In addition, the dielectric is thicker than desired for the channel lengths fabricated to achieve good electrostatics in the device. Control experiments with devices that were immersed into either solely THF or a solution of catechol in THF displayed I/V curves that were similar to the open circuits (I_{SD} approximately pA) and had no gate effect.

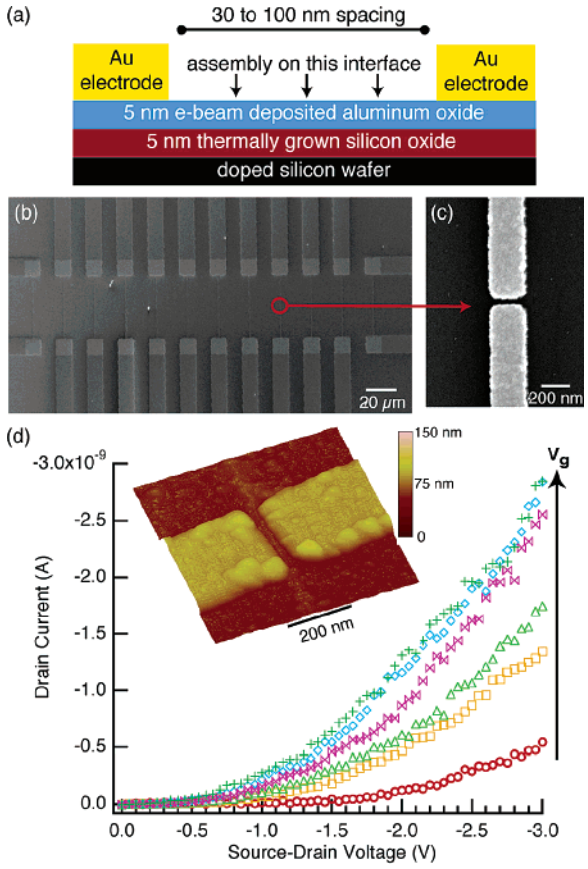

Figure 4. (a) Schematic of the test structure. (b) SEM image. (c) SEM image of the 40 nm gap. (d) Source-drain *I*/*V* curves at different gate biases [$G_V = 0$ (red) to -2.5 V (dark green) in -0.5 steps]. Inset: Tapping mode AFM image of the 40 nm device. The SEM and AFM images are from the device measured in Figure 4d.

In summary, this study puts forth a new class of organic semiconductor that spontaneously forms upright monolayers on gate oxides. When these monolayers are assembled in prefabricated transistor structures, they form the active channel in the device. The path forward to optimize the electronics is tuning the monolayer structure on the gate dielectric surface, reducing the dielectric thickness, and improving the dielectric quality using high-k dielectrics deposited by atomic layer deposition. Concomitant with this strategy is the ability to use the substrate's symmetry and crystallographic space group to control the assembly of the organic semiconductor. Moreover, since the active channel of these devices is exposed to the environment, they could act as highly sensitive environmental and molecular sensors.

Acknowledgment. We acknowledge primary financial support from the Nanoscale Science and Engineering Initiative of the National Science Foundation under NSF Award Number CHE-0117752 and by the New York State Office of Science, Technology, and Academic Research (NYSTAR). We thank T. Graham and IBM's CSS, particularly N. Ruiz, and MRL for metallization, lithography, and silicon fabrication. National Synchrotron Light Source at Brookhaven National Laboratory is supported by the U.S. Department of Energy under Contract No. DE-AC02-98CH10886. C.N. thanks the Beckman Young Investigator Program (2002), the American Chemical Society PRF type G (#39263-G7), the Dupont Young Investigator Program (2002), the Camille Dreyfus Teacher Scholar Program (2004), and the Alfred P. Sloan Fellowship Program (2004). We thank the MRSEC Program of the National Science Foundation under Award Number DMR-0213574 and by the New York State Office of Science, Technology and Academic Research (NYSTAR) for financial support for M.L.S. and the shared instrument facility.

Note Added after ASAP Publication: In the version published on the Web November 2, 2004, there were errors in the caption for Figure 4. The caption to Figure 4 is correct in the final Web version published on November 10, 2004, and in the print version.

Supporting Information Available: Synthetic details and characterization of **1**−**5**. Experimental details for the synchrotron X-ray reflectivity, XPS, RAIRS measurements, and the device preparation/characterization.

References

(1) For a discussion of monolayer transistors, see: Kagan, C. R.; Afzali, A.; Martel, R.; Gignac, L. M.; Solomon, P. M.; Schrott, A. G.; Ek, B. *Nano Lett.* **2003**, *3*, 119.
(2) Dimitrakopoulos, C. D.; Malenfant, P. R. L. *Adv. Mater.* **2002**, *14*, 99.
(3) Katz, H. E.; Bao, Z.; Gilat, S. L. *Acc. Chem. Res.* **2001**, *34*, 359.
(4) Katz, H. E.; Bao, Z. *J. Phys. Chem. B* **2000**, *104*, 671.
(5) Horowitz, G. *Adv. Mater.* **1998**, *10*, 365.
(6) Sandberg, H. G. O.; Frey, G. L.; Shkunov, M. N.; Sirringhaus, H.; Friend, R. H. *Langmuir* **2002**, *18*, 10176.
(7) Horowitz, G.; Peng, X.-Z.; Fichou, D.; Garnier, F. *Synth. Met.* **1992**, *51*, 419.
(8) Ziemelis, K. E.; Hussain, A. T.; Bradley, D. D. C.; Friend, R. H. *Phys. Rev. Lett.* **1991**, *66*, 2231.
(9) Horowitz, G.; Hajlaoui, R.; Bourguiga, R.; Hajlaoui, M. *Synth. Met.* **1999**, 101, 401.
(10) Fritz, S. E.; Martin, S. M.; Frisbie, C. D.; Ward, M. D.; Toney, M. F. *J. Am. Chem. Soc.* **2004**, *126*, 4084.
(11) Meyer zu Heringdorf, F. J.; Reuter, M. C.; Tromp, R. M. *Nature* **2001**, *412*, 517.
(12) Meyer zu Heringdorf, F. J.; Reuter, M. C.; Tromp, R. M. *Appl. Phys. A* **2004**, *A78*, 787.
(13) Weidkamp, K. P.; Hacker, C. A.; Schwartz, M. P.; Cao, X.; Tromp, R. M.; Hamers, R. J. *J. Phys. Chem. B* **2003**, *107*, 11142.
(14) Dodabalapur, A.; Torsi, L.; Katz, H. E. *Science* **1995**, *268*, 270.
(15) Martin, S. T.; Kessselman, J. M.; Park, D. S.; Lewis, N. S.; Hoffman, M. R. *Environ. Sci. Technol.* **1996**, *30*, 2535.
(16) McBride, M. B.; Wesselink, L. G. *Environ. Sci. Technol.* **1988**, *22*, 703.
(17) Moser, J.; Punchihewa, S.; Infelta, P. P.; Gratzel, M. *Langmuir* **1991**, *7*, 3012.
(18) Vasudevan, D.; Stone, A. T. *Environ. Sci. Technol.* **1996**, *30*, 1604.
(19) Conner, P. A.; Dobson, K. D.; McQuillan, A. J. *Langmuir* **1995**, *11*, 4193.
(20) Meng, H.; Bendikov, M.; Mitchell, G.; Helgeson, R.; Wudl, F.; Bao, Z.; Siegrist, T.; Kloc, C.; Chen, C.-H. *Adv. Mater.* **2003**, *15*, 1090−1093.
(21) Luo, J.; Hart, H. *J. Org. Chem.* **1987**, *52*, 4833.
(22) Jung, F.; Molin, M.; Van Den Elzen, R.; Durst, T. J. *J. Org. Chem.* **1974**, *96*, 935.
(23) Jarvis, W. F.; Hoey, M. D.; Finocchio, A. L.; Dittmer, D. C. *J. Org. Chem.* **1988**, *53*, 5750.
(24) Askari, S.; Lee, S.; Perkins, R. R.; Scheffer, J. R. *Can. J. Chem.* **1985**, *63*, 3526.
(25) Martin, N.; Behnisch, R.; Hanack, M. J. *J. Org. Chem.* **1989**, *54*, 2563.
(26) The assembly of **1** was screened against the metal oxides from a millimolar solution in THF. Substrates were cleaned via UV-ozone treatment prior to deposition. Following deposition, the samples were placed in fresh THF to remove any unbound molecules.
(27) The wavelength of the synchotron radiation was 1.208 Å.
(28) The surface is modeled as an overlayer of tetracene on top of the more electron dense aluminum oxide substrate. As shown in Figure 1, the hydroxyl groups are incorporated into the substrate, thus the transition to the lower electron density overlayer begins with the tetracene core.
(29) Baptiste, A.; Gibaud, A.; Bardeau, J. F.; Wen, K.; Moaz, R.; Sagiv, J.; Ocko, B. M. *Langmuir* **2002**, *18*, 3916.
(30) Gibaud, A. In *X-ray and Neutron Reflectivity: Principle and Applications*; Daillant, J., Gibaud, A., Eds.; Springer: Paris, 1999.
(31) The fit was generated by a least-squares method. The surface roughness for both interfaces is 2.8 ± 0.1 Å.
(32) Since the transition to lower electron density occurs at the carbon of the tetracene core, the height of the molecule was calculated as the length of the molecule from the first aromatic carbon to the terminal hydrogens.
(33) The electron density is calculated from the bulk density and the number of electrons per molecule.
(34) See the Supporting Information for the XPS data.
(35) A quinone would result in a C_{1s} peak shift of approximately 4 eV.
(36) Since RAIRS uses p-polarized light, the upright orientation is further supported by the presence of the aromatic vibrational frequencies.
(37) Urban, M. W. *Vibrational Spectroscopy of Molecules and Macromolecules on Surfaces*; John Wiley & Sons: New York, 1993; p 73.
(38) Franssila, S.; Paloheimo, J.; Kuivalainen, P. *Electron. Lett.* **1993**, *29*, 713.
(39) Collet, J.; Tharaud, O.; Chapoton, A.; Vuillaume, D. *Appl. Phys. Lett.* **2000**, *76*, 1941.
(40) Austin, M. S.; Chou, S. Y. *Appl. Phys. Lett.* **2002**, *81*, 4431.
(41) Zhang, Y.; Petta, J. R.; Ambily, S.; Shen, Y.; Ralph, D. C.; Malliaras, G. G. *Adv. Mater.* **2003**, *15*, 1632.

JA044101Z